Weierstraß-Institut
für Angewandte Analysis und Stochastik

im Forschungsverbund Berlin e.V.

Preprint ISSN 0946 – 8633

Analyzing fMRI experiments with structural adaptive smoothing procedures

Karsten Tabelow[1] [2], Jörg Polzehl[1], and Vladimir Spokoiny[1]

submitted: 20th December 2005

[1] Weierstrass Institute
for Applied Analysis and Stochastics,
Mohrenstr. 39, 10117
Berlin, Germany
E-Mail: tabelow@wias-berlin.de

No. 1079

Berlin 2005

[2]Supported by the DFG Research Center MATHEON "Mathematics for key technologies" in Berlin

2000 *Mathematics Subject Classification.* 62P10, 92C55, 62G05, 62G10 .

Key words and phrases. functional MRI, spatially adaptive smoothing, signal detection.

Edited by
Weierstraß-Institut für Angewandte Analysis und Stochastik (WIAS)
Mohrenstraße 39
10117 Berlin
Germany

Fax: + 49 30 2044975
E-Mail: preprint@wias-berlin.de
World Wide Web: http://www.wias-berlin.de/

Abstract

Data from functional magnetic resonance imaging (fMRI) consists of time series of brain images which are characterized by a high noise level and a low signal-to-noise ratio. We provide a complete procedure for fMRI analysis. In order to reduce noise and to improve signal detection the fMRI data is spatially smoothed. However, the common application of a Gaussian filter does this at the cost of loss of information on spatial extend and shape of the activation area. We suggest to use the propagation-separation procedures introduced by Polzehl and Spokoiny (2005) instead. We show that this significantly improves the information on the spatial extend and shape of the activation region with similar results for the noise reduction. Signal detection is based on locally varying thresholds defined by random field theory. Effects of adaptive and non adaptive smoothing are illustrated by artificial examples and an analysis of real data.

1 Introduction

Functional Magnetic Resonance Imaging (fMRI) is a non-invasive tool for studying the functionality of the brain and localizing cognitive functions. It has become increasingly important in neurosciences as well as for clinical applications such as presurgical planning. In a typical fMRI experiment with block design the patient has to perform one or several tasks alternated by some period of rest. However, activation in brain is not subject to direct measurement. fMRI-experiments therefore detect a change in blood oxygenation (BOLD response) Lange (1996); Lange and Zeger (1997) instead. A higher oxygenation level is associated with increased neuronal activity necessary to solve the task.

fMRI data is obtained as time series of three dimensional images. It is characterized by a high noise level and a very low signal-to-noise ratio. The spatial resolution (voxel size) is typically of the order of $3-4$mm. The time series can be as long as $T = 100$ to $T = 1000$ scans with a repetition time of typically 2 or 3 seconds. The data is correlated in space and time.

In this paper we adopt the common view of a linear model for the time series $Y_i = (Y_{it})$ in each voxel i Worsley et al. (2002):

$$Y_i = X\beta_i + \varepsilon_i. \tag{1}$$

Here, X denotes the design matrix. The first columns of X correspond to the experimental stimuli and contain the expected BOLD responses connected with the tasks. Other columns contain variables to model orthogonal effects such as drift or signals from heartbeat and breathing. The errors $\varepsilon_i = (\varepsilon_{it})$ are correlated in space and time. The parameter vector β_i is to be estimated. Interest usually is in one of the parameters associated with a stimulus in the experiment or in a contrast $\gamma_i = c^T\beta_i$, i.e. a linear combination of such parameters. More sophisticated non-linear models also exist Purdon et al. (2001) but will not be considered in this paper.

In activated voxel we expect the parameter of interest or contrast $\gamma_i = c^T\beta$ to differ significantly from zero. We may therefore test the hypotheses H: $\gamma_i = 0$ against an alternative A: $\gamma_i \neq 0$. This induces a severe multiple test problem. A voxelwise analysis, using individual critical values, produces a large portion of false positive signals. At the same time small signals are concealed due to high variability of the parameter estimates. The use of a global critical value, i.e. specification of an error probability to observe a false positive in any voxel, usually leads to no signal detection at all.

One solution is to smooth the parameter array. This reduces variability, while the mean value is preserved in spatially extended regions with similar values of γ. At the same time a correlation structure is induced in the three-dimensional parameter field $\Gamma = \{\gamma_i\}$, $i = (i_x, i_y, i_z)$, that allows for much lower global thresholds. However, application of commonly used methods, like e.g. a Gaussian filter, achieves this at the cost of loss of information on spatial extend and shape of the activation areas. According to the matched filter theorem Rosenfeld and Kak (1982); Worsley et al. (1996a) the bandwidth of a non adaptive Gaussian filter is best chosen as the expected size of the (usually unknown) activation areas.

In contrast a spatially adaptive method like adaptive weights smoothing (AWS), suggested in Polzehl and Spokoiny (2000), naturally adapts to the sizes and shapes of the activated areas rather than over-smoothing them. For theoretical results on a generalization of this method, the Propagation-Separation (PS) approach, we refer to Polzehl and Spokoiny (2005). In this paper we suggest to apply a spatially adaptive smoothing procedure in the analysis of fMRI experiments and show how it improves the inferred information on the spatial extend and shape of the activated regions.

The use of such an idea for fMRI analysis has already been suggested in Polzehl and Spokoiny (2001). However, Polzehl and Spokoiny (2001) left several important questions open. The approach was restricted to periodic activations. Furthermore it did not consider temporal and spatial correlation present in the data. And finally it failed to provide a

formal solution to select appropriate thresholds for signal detection. In this paper we will overcome all these drawbacks and provide a complete procedure for structurally adaptive fMRI analysis using the PS approach.

The paper is organized as follows. In Section 2 we describe the estimation of the parameters β_i in our analysis. This includes the description of the linear model (1) and the prewhitening used to account for the temporal autocorrelation. After voxelwise estimation of β_i we apply a Propagation-Separation procedure to the map of contrasts $\Gamma = \{\gamma_i\}$. We then define thresholds for signal detection using Random Field Theory, see Worsley (1994); Worsley et al. (1996b). Details of the procedure are outlined in Section 3. In Section 4 we illustrate the application of the procedure to real fMRI data as well as artificial examples to underline the advantages of the method in different situations. Section 5 gives a summary.

2 Voxelwise analysis of time series

In fMRI the BOLD effect is used as a natural contrast employing the fact that voxel with increased neuronal activity are characterized by a higher oxygenation level. The expected BOLD response can be modeled by a convolution of the task indicator function with the hemodynamic response function. This function has been measured Glover (1999) and models the fact that although neuronal activation is thought to be practically instantaneous to the stimulus, blood oxygenation is subject to some delay and shows a more complicated structure than a simple indicator function. In fMRI experiments one finds a characteristic form for the measured BOLD response. Several suggestions have been made to model the hemodynamic response function $h(t)$. We follow Worsley et al. (2002) and give the $h(t)$ as the difference of two gamma functions Glover (1999):

$$h(t) = \left(\frac{t}{d_1}\right)^{a_1} \exp\left(-\frac{t-d_1}{b_1}\right) - c\left(\frac{t}{d_2}\right)^{a_2} \exp\left(-\frac{t-d_2}{b_2}\right)$$

with $a_1 = 6$, $a_2 = 12$, $b_1 = 0.9$, $b_2 = 0.9$, and $d_i = a_i b_i$, $c = 0.35$ where t is the time in seconds.

Given the stimulus $s(t)$ as a task indicator function, we arrive at the expected BOLD response as convolution of $s(t)$ and $h(t)$:

$$x(t) = \int_0^\infty h(u)s(t-u)du.$$

The resulting function $x(t)$ is evaluated at the T scan acquisition times t_k. Fig. 1 illustrates the function $x(t)$ for a typical experimental design.

We consider the linear model (1) for the time series Y_i in each voxel i after reconstruction of the raw data and motion correction. The first q columns of X contain values of the

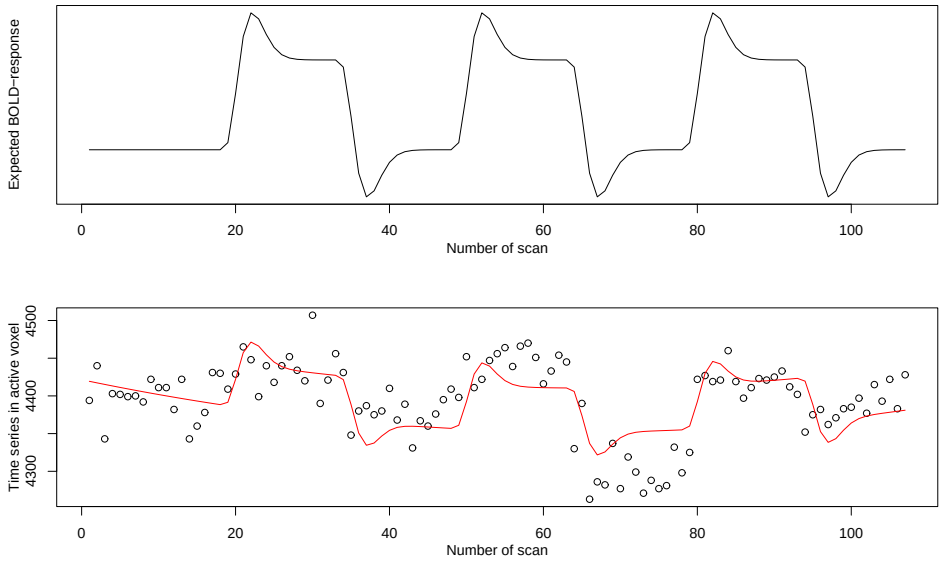

Figure 1: Upper: BOLD response for a stimulus at three onset times given in scans. Lower: Data and fit using the linear model (1) in one voxel . We account for the BOLD response as well as some slow drift terms that can be well approximated by polynomials. Data: H. Voss, Citigroup Biomedical Imaging Center, Weill Medical College of Cornell University

expected BOLD response for the different stimuli evaluated at scan acquisition times. The other $p - q$ columns are chosen to be orthogonal to the expected BOLD responses and to account for a slowly varying drift and possible other external effects, see Worsley et al. (2002). The error vector ε_i has zero expectation and is assumed to be correlated in time. In order to access the variability of the estimates of β_i correctly we have to take the correlation structure of the error vector ε_i into account. Here we follow Worsley et al. (2002); Worsley (2005) assuming an AR(1) model to be sufficient for commonly used MRI scanners. The autocorrelation coefficients ρ_i are estimated from the residual vector $r_i = (r_{i1}, \ldots, r_{iT})$ of the fitted model (1) as

$$\overline{\rho}_i = \sum_{t=2}^{T} r_{it} r_{i(t-1)} / \sum_{t=1}^{T} r_{it}^2.$$

This estimate of the correlation coefficient is biased due to fitting the linear model (1) Worsley et al. (2002). We therefore apply the bias correction given by Worsley et al. (2002) leading to an estimate $\widetilde{\rho}_i$.

We then use prewhitening to transform model (1) into a linear model with approximately independent errors. The prewhitened linear model is obtained by multiplying the terms in (1) with some matrix A_i depending on $\widetilde{\rho}_i$, see Worsley et al. (2002). The prewhitening

procedure thus results in a new linear model

$$\widetilde{Y}_{it} = \widetilde{X}_i \beta_i + \widetilde{\varepsilon}_{it} \tag{2}$$

with $\widetilde{Y}_i = A_i Y_i$, $\widetilde{X}_i = A_i X$, and $\widetilde{\varepsilon}_i = A_i \varepsilon_t$. In the new model the distribution of the errors $\widetilde{\varepsilon}_{it}$ are approximately independent in t, such that $\operatorname{Var} \varepsilon_i = \sigma_i^2 I_T$.

Finally parameter estimates $\widetilde{\beta}_i$ are obtained by least squares from model (2) as

$$\widetilde{\beta} = (\widetilde{X}^T \widetilde{X})^{-1} \widetilde{X}^T \widetilde{Y}.$$

The error variance σ_i^2 is estimated from the residui $\widetilde{r}_i$ of the linear model (2) as $\widetilde{\sigma}_i^2 = \sum_1^T \widetilde{r}_{it}^2/(T-p)$ leading to estimated covariance matrices

$$\operatorname{Var} \widetilde{\beta} = \widetilde{\sigma}^2 (\widetilde{X}^T \widetilde{X})^{-1}.$$

This leaves us with three dimensional arrays $\widetilde{\Gamma}$, $\widetilde{S}$ containing the estimated contrasts $\widetilde{\gamma}_i = c^T \widetilde{\beta}_i$ and their estimated standard deviations $\widetilde{s}_i = (c^T \operatorname{Var} \widetilde{\beta}_i c)^{1/2}$. The voxelwise quotient $\widetilde{\theta}_i = \widetilde{\gamma}_i / \widetilde{s}_i$ of both arrays forms a statistical parametric map (SPM) $\widetilde{\Theta}$. This map is approximately a random t-field, see Worsley (1994). All arrays carry a correlation structure induced by the spatial correlation in the fMRI data.

3 Spatial smoothing and signal detection

A voxelwise signal detection may now be based on the statistical parametric map (SPM) Θ, i.e. define a voxel as activated if the corresponding value in the statistical parametric map (SPM) Θ exceeds a critical value or threshold. Such an analysis is inefficient in the sense that it either produces a large number of false positive signals or fails to detect many of the activations. The first situation is typical for applying a voxelwise threshold to the large number of voxel in the data cube while the second case is characteristic if thresholds are controlled by a global significance level. Both sensitivity and specitivity of signal detection can be considerably improved by spatial smoothing of the array $\widetilde{\Gamma}$.

Usually spatial smoothing is applied to the original images in the fMRI time series prior to parameter estimation in the linear model. We note that for parameter estimation, except for effects from prewhitening, the order in which nonadaptive spatial smoothing and evaluation of the linear model are performed is arbitrary. If temporal correlations are spatially homogeneous temporal and spatial smoothing can be interchanged. If temporal correlation are estimated both alternatives deliver similar results, with probably higher bias and less variance if spatial smoothing is performed first. Nevertheless smoothing the

contrasts $\widetilde{\gamma}_i$ obtained from the original fMRI data allows for a much better assessment for the variance of $\widehat{\gamma}_i$, see Subsection 3.5.

For spatial adaptive smoothing the order of both steps is important. The quality of adaptation heavily depends on the signal to noise ratio present in the data. Parameter estimation in the linear model serves as a variance and dimension reduction step prior to spatial smoothing and therefore allows for a much better adaptation.

We propose to use a spatial adaptive smoothing procedure based on the Propagation-Separation approach from Polzehl and Spokoiny (2005) on the array of estimated parameters.

3.1 Propagation-Separation approach

We shortly explain the main idea. Let us assume that for each voxel with coordinates $i = (i_x, i_y, i_z)$ the parameter γ can be well approximated by a constant within a local vicinity $U(i)$ of voxel i. This serves as our structural assumption.

Our estimation problem can now be viewed as consisting of two parts. In order to efficiently estimate the parameter γ_i in a voxel i we need to describe a local model, i.e. to assign weights $W_i = \{w_{i1}, \ldots, w_{in}\}$. If we knew the neighborhood $\mathcal{U}(i)$ we would define local weights as $w_{ij} = I_{j \in \mathcal{U}(i)}$ and use the weighted least squares estimate

$$\widehat{\gamma}_i = \sum_j \widetilde{w}_{ij} \widetilde{\gamma}_j / \sum_j \widetilde{w}_{ij} \quad \text{with} \quad \widetilde{w}_{ij} = w_{ij} / \widetilde{s}_j^2 \tag{3}$$

as an estimate of γ_i. Since γ_i and therefore $\mathcal{U}(i)$ are unknown the assignments will have to depend on the information on Γ that we can extract from the estimates in $\widetilde{\Gamma}$ and their estimated variances. If we have good estimates $\widehat{\gamma}_j$ of γ_j we can use this information to infer on the set $\mathcal{U}(i)$ by testing the hypothesis

$$H : \gamma_j = \gamma_i. \tag{4}$$

A weight w_{ij} can be assigned based on the value of a test statistic T_{ij}, assigning zero weights if $\widehat{\gamma}_j$ and $\widehat{\gamma}_i$ are significantly different. This provides us with a set of weights $W_i = \{w_{i1}, \ldots, w_{in}\}$ that determines a local model in voxel i. These weights can then be used to obtain new estimates of the parameter function γ in each voxel i by (3).

We utilize both steps in an iterative procedure. We start with a very local model in each voxel i given by weights

$$w_{ij}^{(0)} = K_{\mathrm{loc}}(\Delta(i, j, h^{(0)})),$$

where $\Delta(i,j,h) = ((i_x - j_x)^2/h_x^2 + (i_y - j_y)^2/h_y^2 + (i_z - j_z)^2/h_z^2)^{1/2}$ is a weighted distance between voxel i and j. The initial vector of bandwidths $h^{(0)} = (h_x^{(0)}, h_y^{(0)}, h_z^{(0)})$ is chosen very small, with its components indirect proportional to the size of a voxel in the three coordinate directions. K_{loc} is a 3D Gaussian kernel with $FWHM = 1$, truncated at $4/\sqrt{8\ln 2}$, i.e. $K_{\text{loc}}(x) = e^{-4\ln 2 x^2} I_{x \le 4/\sqrt{8\ln 2}}$. Except from truncation this is the common choice in the fMRI and random fields literature and used here for comparability.

We then iterate two steps, estimation of Γ and refining the local models. In the kth iteration new weights are generated as

$$w_{ij}^{(k)} \quad = \quad K_{\text{loc}}(\Delta(i,j,h^{(k)}))K_{\text{st}}(\boldsymbol{\zeta}_{ij}^{(k)}) \quad \text{with} \quad \boldsymbol{\zeta}_{ij}^{(k)} = T_{ij}^{(k)}/\lambda \quad \text{and} \quad K_{\text{st}}(x) = e^{-x} I_{x<5}.$$

The bandwidth $h^{(k)}$ is increased by a constant factor with each iteration k. The term

$$T_{ij}^{(k)} = N_i^{(k-1)}(\widehat{\gamma}_i^{(k-1)} - \widehat{\gamma}_j^{(k-1)})^2$$

with $N_i^{(k-1)} = \sum_j \widetilde{w}_{ij}^{(k-1)}$ is used to specify the penalty $\boldsymbol{\zeta}_{ij}^{(k)}$, see Polzehl and Spokoiny (2005). Then we recompute the estimates employing the just defined weights as

$$\widehat{\gamma}_i^{(k)} = \frac{1}{N_i^{(k)}} \sum_j \widetilde{w}_{ij}^{(k)} \widetilde{\gamma}_j$$

where $\widetilde{w}_{ij}^{(k)} = w_{ij}^{(k)}/\widetilde{s}_j$ and $N_i^{(k)} = \sum_j \widetilde{w}_{ij}^{(k)}$.

Without spatial correlation $\widehat{\gamma}_i^{(k)}$ has variance

$$V_i^{(k)} = Q_i^{(k)}/(N_i^{(k)})^2 \le 1/N_i^{(k)} \quad \text{with} \quad Q_i^{(k)} = \sum_j (\widetilde{w}_{ij}^{(k)})^2 \widetilde{s}_j^2,$$

i.e. the term $1/N_i^{(k)}$ approximately reflects the variability of $\widehat{\gamma}_i^{(k)}$.

3.2 Correction for spatial correlation

In our situation we have to adjust for the spatial correlation present in the data. The correlation in each direction is estimated as a global value using the residuals from model (2). This may also be done locally, see e.g. Kiebel et al. (1999).

Let us assume that the spatial correlation present in $\widetilde{\Gamma}$ results from spatial smoothing using the location kernel K_{loc} and employing bandwidths $g = (g_x, g_y, g_z)$ in the three coordinate directions. This means that, for a interior voxel i, we assume the elements of $\widetilde{\Gamma}$ to be generated from a spatially uncorrelated field $\check{\Gamma}$ with $Var\check{\gamma}_l = \check{s}_l^2$ as

$$\widetilde{\gamma}_i = \sum_j K_{\text{loc}}(\Delta(i,j,g))\check{\gamma}_j / N_g \quad \text{with} \quad N_g = \sum_j K_{\text{loc}}(\Delta(i,j,g)).$$

This results in

$$\widehat{\gamma}_i^{(k)} = \frac{1}{N_i^{(k)} N_g} \sum_j \widetilde{w}_{ij}^{(k)} \sum_l K_{\mathrm{loc}}(\Delta(j,l,g)) \check{\gamma}_l$$

Then the variance of $\widehat{\gamma}_i^{(k)}$ is given by

$$\begin{aligned} \widehat{V}_i^{(k)} &= \frac{\sum_l \check{s}_l^2 \big[\sum_j \widetilde{w}_{ij}^{(k)} K_{\mathrm{loc}}(\Delta(j,l,g))\big]^2}{(N_i^{(k)})^2 N_g^2} \\ &= \frac{\sum_l \check{s}_l^2 \big[\sum_j \widetilde{w}_{ij}^{(k)} K_{\mathrm{loc}}(\Delta(j,l,g))\big]^2}{\sum_j (\widetilde{w}_{ij}^{(k)})^2 \widetilde{s}_j^2 N_g^2} V_i^{(k)} \end{aligned}$$

Let $Q_g = \sum_j K_{\mathrm{loc}}(\Delta(i,j,g))^2$. Note that, except at the boundaries of the data cube, the sums Q_g and N_g do not depend on the voxel i. Then for spatially homogeneous variances $\check{s}_l^2 \equiv \check{s}^2$, i.e. $\widetilde{s}_i^2 = Q_g / N_g^2 \check{s}^2$,

$$\widehat{V}_i^{(k)} \approx \frac{\sum_l \big[\sum_j \widetilde{w}_{ij}^{(k)} K_{\mathrm{loc}}(\Delta(j,l,g))\big]^2}{\sum_j (\widetilde{w}_{ij}^{(k)})^2 Q_g} V_i^{(k)}.$$

If the statistical penalty is negligible, i.e. $w_{ij}^{(k)} \approx K_{\mathrm{loc}}(\Delta(i,j,h^{(k)}))$ then

$$\begin{aligned} \widehat{V}_i^{(k)} &\approx \frac{\sum_l \big[\sum_j K_{\mathrm{loc}}(\Delta(i,j,h^{(k)})) K_{\mathrm{loc}}(\Delta(j,l,g))\big]^2}{\sum_j K_{\mathrm{loc}}^2(\Delta(i,j,h^{(k)})) Q_g} V_i^{(k)} \\ &= C(g,h^{(k)}) V_i^{(k)}. \end{aligned}$$

The factor $C(g,h^{(k-1)})^{-1}$ will be used as an adjustment to $N_i^{(k-1)}$ in the definition of $T_{ij}^{(k)}$ to account for spatial correlation.

3.3 Propagation-Separation algorithm for heteroscedastic correlated data

We now formally describe the resulting algorithm.

- **Initialization:** Set the initial bandwidth $h^{(0)}$ and compute, for every i, the statistics

  $$N_i^{(0)} = \sum_j K_{\mathrm{loc}}(\Delta(i,j,h^{(0)}))/\widetilde{s}_j^2, \quad \text{and} \quad U_i^{(0)} = \sum_j K_{\mathrm{loc}}(\Delta(i,j,h^{(0)}))\widetilde{\gamma}_j/\widetilde{s}_j^2$$

  and the estimates

  $$\widehat{\gamma}_i^{(0)} = U_i^{(0)}/N_i^{(0)}.$$

  Set $k = 1$ and $h^{(1)} = c_h h^{(0)}$ for some $c_h > 1$.

- **Adaptation:** For every pair i, j, compute the penalty

$$\begin{aligned}\boldsymbol{\zeta}_{ij}^{(k)} &= (\lambda C(g, h^{(k-1)})^{-1} T_{ij}^{(k)} \\ &= (\lambda C(g, h^{(k-1)})^{-1} N_i^{(k-1)} (\widehat{\theta}_i^{(k-1)} - \widehat{\theta}_j^{(k-1)})^2.\end{aligned}$$

  Compute weights $w_{ij}^{(k)}$ as

$$w_{ij}^{(k)} = K_{\mathrm{loc}}\big(\Delta(i, j, h^{(k)})\big) K_{\mathrm{st}}\big(\boldsymbol{\zeta}_{ij}^{(k)}\big) \quad \text{and} \quad \widetilde{w}_{ij}^{(k)} = w_{ij}^{(k)} / \widetilde{s}_j^2.$$

- **Local estimation:** Now compute new local MLE estimates $\widetilde{\gamma}_i^{(k)}$ of γ_i as

$$\widehat{\gamma}_i^{(k)} = U_i^{(k)} / N_i^{(k)} \qquad \text{with} \qquad N_i^{(k)} = \sum_j \widetilde{w}_{ij}^{(k)}, \quad U_i^{(k)} = \sum_j \widetilde{w}_{ij}^{(k)} \widetilde{\gamma}_j \,.$$

- **Stopping:** Stop if $h_x^{(k)} \geq h_{\max}$, otherwise set $h^{(k)} = c_h h^{(k-1)}$, increase k by 1 and continue with the adaptation step.

An estimate of the variance of the final estimate $\widehat{\gamma}_i^{(k^*)}$ is given by

$$\widehat{s}_i^2 = \widehat{V}_i^{(k^*)} = C(g, h^{(k^*)}) Q_i^{(k^*)} / (N_i^{(k^*)})^2 \quad \text{with} \quad Q_i^{(k^*)} = \sum_j (\widetilde{w}_{ij}^{(k^*)})^2 \widetilde{s}_j^2$$

3.4 Choice of parameters - Propagation condition

The proposed procedure involves several parameters. The most important one is the scale parameter λ in the statistical penalty $\boldsymbol{\zeta}_{ij}$. The special case $\lambda = \infty$ simply leads to a kernel estimate with bandwidth $h_{\max}$. We propose to chose λ as the smallest value satisfying a propagation condition. This condition requires that, if the local assumption is valid globally, i.e. $\gamma_i \equiv \gamma$ does not depend on i, then at each step of the algorithm the adaptive estimate approximately behaves like its non-adaptive counterpart that employs the same bandwidth. Particularely the final estimate for $h_{\max} = \infty$ has approximately the same quality as the global estimate. More formally we request that in this case for each k

$$\boldsymbol{E}|\widehat{\gamma}^{(k)} - \gamma| < (1 + \alpha) \boldsymbol{E}|\check{\gamma}^{(k)} - \gamma| \tag{5}$$

for a specified constant $\alpha > 0$. Here

$$\check{\gamma}_i^{(k)} = \frac{\sum_j K_{\mathrm{loc}}(\Delta(i, j, h^{(k)}))/\widetilde{s}_j^2 \widetilde{\gamma}_j}{\sum_j K_{\mathrm{loc}}(\Delta(i, j, h^{(0)}))/\widetilde{s}_j^2}$$

denotes the nonadaptive kernel estimate employing the bandwidth $h^{(k)}$ from step k. The value λ provided by this condition does not depend on the unknown model parameter γ

and can therefore be approximately found by simulations. We set a default value for λ using $\alpha = 0.1$.

The second parameter of interest is the maximal bandwidth $h_{\max}$ which controls both numerical complexity, i.e. the number of iterations k^*, of the algorithm and smoothness within homogeneous regions.

The initial bandwidth is chosen as $h^{(0)} = v_x/\sqrt{8\ln 2}/(v_x, v_y, v_z)$ in units of $v_x mm$. The bandwidth is increased after each iteration by a default factor $c_h = 1.25^{1/3}$.

Choosing parameters in this procedure by the propagation condition (5) ensures the algorithm to behave like a corresponding non-adaptive smoothing algorithm in large homogeneous regions. We conclude, that the maximum bandwidth of the kernel used in the iterative procedure can be chosen as FWHM of 2-3 times voxel size as usual. In the statistical map the largest homogeneous region is formed by voxel in areas not related to the experiments, while smaller regions correspond to areas of activation, that are characterized by values of β different from zero. Therefore under the hypothesis H: $\beta = 0$ the AWS procedure approximately behaves like the non-adaptive smoothing procedure. This is important for the definition of the thresholds using Random Field Theory. At the same time the separation property of AWS allows to clearly separate activated areas from regions not affected by the experiment.

3.5 Properties of $\widehat{\Gamma}$ and $\widehat{S}$

Adaptive spatial smoothing results in arrays $\widehat{\Gamma} = (\widehat{\gamma}_i)$ and $\widehat{S} = (\widehat{s}_i)$. If no activation is present in any voxel, i.e the hypothesis H: $\gamma_i = 0$ holds for all i, choosing the smoothing parameter λ by the propagation condition (5) ensures the properties of $\widehat{\Gamma}$ and $\widehat{S} = (\widehat{s}_i)$ to approximately coincide with properties of the corresponding arrays obtained by nonadaptive smoothing employing the kernel $K_{\rm loc}$ with bandwidth h_{max}.

We now shortly explain the effect of spatial smoothing on properties of $\widehat{S} = (\widehat{s}_i)$. Let us assume that $S^2 = (s_i^2)$ is an array of i.i.d. χ^2 variables with d_f degrees of freedom. Let weights w_{ij} be fixed. Then the distribution of

$$C_s \overline{s}_i = C_s \frac{\sum_j w_{ij}^2 s_j^2}{(\sum_j w_{ij})^2}$$

with $C_s = \frac{\sum_j w_{ij}^2 (\sum_j w_{ij})^2}{\sum_j w_{ij}^4}$ can be well approximated by a χ^2-distribution with $\frac{(\sum_j w_{ij}^2)^2}{\sum_j w_{ij}^4} d_f$ degrees of freedom. A similar behavior is, for sufficiently lage d_f, observed for

$$\widetilde{C}_s \widehat{s}_i = \widetilde{C}_s \frac{\sum_j \widetilde{w}_{ij}^2 s_j^2}{(\sum_j \widetilde{w}_{ij})^2}$$

with $\widetilde{C}_s$ depending on both d_f and the weighting scheme. We see that the degrees of freedom for $\widehat{S}$ increase with its smoothness induced by spatial smoothing. Note that this is in strict contrast to the situation where spatial smoothing is applied to the original observed images prior to estimation of parameters in the linear model (1), in which case the degrees of freedom are not affected by the spatial smoothing.

Adaptive smoothing leads to a different weighting scheme in each voxel resulting in spatially varying smoothness of $\widehat{\Gamma}$ and $\widehat{S}$ and spatially varying degrees of freedom in the distribution $\widehat{s}_i$. On the other side spatial smoothing leads, in each voxel, to a sufficient number of degrees of freedom, allowing to approximate the distribution of the array $\widehat{\Theta} = (\widehat{\gamma}_i/\widehat{s}_i)$ by a (spatially inhomogeneous) Gaussian field.

3.6 Spatial inhomogeneity

In case of non-adaptive smoothing, e.g. $\lambda = \infty$, and homogeneous variance the spatial correlation in this field can be characterized by a FWHM bandwidth h^{Gauss} of a Gaussian kernel that leads to a variance reduction by a factor of

$$F_i^{Gauss} = \frac{\sum_k \left[\sum_j K_{\mathrm{loc}}(\Delta(i,j,h_{\max}))K_{\mathrm{loc}}(\Delta(j,k,g))\right]^2}{N_{h_{max}}^2 N_g^2}. \tag{6}$$

Under the assumption $\gamma \equiv 0$ spatial adaptive smoothing by our Propagation-Separation procedure, see Subsection 3.3, leads, due to the propagation condition (5), to an approximately homogeneous field. Local spatial correlation can again be viewed as resulting from non-adaptive spatial smoothing with a FWHM h_i^{PS} that yields a variance reduction by

$$F_i^{PS} = \frac{\sum_k \left[\sum_j \widetilde{w}_{ij}^{(k^*)} K_{\mathrm{loc}}(\Delta(j,k,g))\right]^2}{(N_i^{(k^*)})^2 N_g^2}.$$

This factor differs from (6) in the sense that it incorporates both spatially varying variances $\widetilde{s}^2$ and spatial inhomogeneity caused by randomness of weights $w_{ij}^{(k^*)}$.

It also reflects the spatially varying smoothness caused by adaptation of weights to the underlying structure in Γ, i.e. a possibly lower smoothness in activated areas.

3.7 Defining p-values

To define appropriate thresholds we follow the argumentation in Worsley (1994) and Worsley et al. (1996a). For a spatially homogeneous Gaussian random field with smoothness $h = (h_x, h_y, h_z)$ in the coordinate directions, measured in FWHM, an appropriate threshold for signal detection can be defined approximating the p-value of an extreme event by

its expected Euler characteristic (EC). Worsley et al. (1996a) shows that an approximate P-value of the maximum Z of a 3D Gaussian random field over a specified search region is given by

$$P(Z > z) \approx \sum_{d=0}^{3} R_d(V, h)\rho_d(z) \tag{7}$$

where R_d is the d-dimensional resel count depending on the volume V of the search region and the smoothness measured by the FWHM bandwidths h in mm, see Worsley (1994). $\rho_d(z)$ is the d-dimensional EC density, see Worsley et al. (1996a) for the case of a Gaussian random field.

The definition of an approximate P-value, simultaneous over the search region, heavily depends on the assumption of stationarity of the random field, see e.g. Worsley (2002); Worsley et al. (1999).

We take a slightly different approach. We first note that for a large search volume the term for $d = 3$ clearly dominates in (7). This means that the exceedance probability $P(Z > z)$ approximately equals to the product of the 3-dimensional resel count and the value of the 3-dimensional EC density at z. In a homogeneous field the first factor $R_3(V, h) = (x-1)\,(y-1)\,(z-1)\,\frac{v_x\,v_y\,v_z}{h_x\,h_y\,h_z}$ is proportional to the size of the search volume and indirect proportional to $h_x h_y h_z$. Here x,y and z are the extensions of the search region in voxel and v_x,v_y and v_z determine the size of a voxel in mm. The value of the 3-dimensional EC density $\rho_3(z)$ efficiently measures the exceedance probability per resolution element, which is spread over a volume of $R_3(V)$ such elements.

For a random field with spatially inhomogeneous smoothness we may consider the search volume to consist of resolution elements of different size, depending on the local smoothness. This yields simultaneous local exceedance probabilities as

$$P(Z_i > z) \approx \sum_{d=0}^{3} R_d(V, h_i)\rho_d(z) \tag{8}$$

with $R_d(V, h_i)$ reflecting the local smoothness. This construction evenly distributes probability mass over the search volume V at the cost of spatially varying thresholds.

Signal detection is now performed for the random field $\widehat{\Theta}$ based on the approximate p-values

$$p_i = \sum_{d=0}^{3} R_d(V, h_i)\rho_d(\widehat{\theta}_i). \tag{9}$$

4 Application of the procedure

In this section we demonstrate various aspects of the procedure introduced in the preceeding Sections in a series of examples.

4.1 Application to artificial data

We first start with an examination of artificial data to show the difference between the use of adaptive and non adaptive smoothing methods in a known situation. We use a typical dimension of $64 \times 64 \times 26$ voxel for the datacube. The activation area consists of voxel with a distance between 5 and 7.5 or 10.5 to 12 from the center of the cube. No activation is assigned to voxel in the two central vertical slices, which induces gaps of width 2 between activation areas (see left image in Figure 2 to view the activation area in a central slice). At each of these voxel a time series of 107 scans is created following an expected BOLD response as shown in Figure 1. The BOLD response is generated using a convolution of the hemodynamic response function with a task indicator function with onset times at scans 18, 48, and 78, and a duration time of 15 scans. Heavy autocorrelated noise following an AR(1) model with an autocorrelation parameter of 0.3 is added at every voxel. In a second analysis we modify the signal to vary smoothly in radial direction. This models the fact that blood oxygenation level increases at different scales in the environment of the activation area due to blood flow. The results of an analysis using a FWHM bandwidth of $h_{max} = 3.05 v_x$ of this data are shown in Figure 2.

The adaptive smoothing procedure leads to a much better signal detection. In order to discuss this in more detail we show, how the detection depends on the signal strength and shape of the activation area. Four different kinds of areas are used: an ellipsoid with principal axis 1.5 and 3, a sphere with radius 2, a cube of size 3, and the configuration used in Figure 2, respectively. We generate an artificial SPM $\widetilde{\Theta}$ of estimated parameters for the BOLD-response as signal plus standard normal noise. Furthermore we assign χ^2_T $T = 100$ random variates to resemble variances of the estimated parameters.

In Figure 3 signal detection using adaptive (PS) and non adaptive smoothing is compared. We vary the assigned signal size in the activation area from 0.6 to 5. This is shown on the x-axis of the diagrams. The number of detected voxel is increasing with the signal size with both methods. However, the analysis using adaptive smoothing is capable to detect smaller signals. Furthermore, while the number of false positive detected voxel is practically zero, for gaussian filtering the number of false positives increases with signal size. The adaptive smoothing method naturally adapt to the different sizes and shapes of

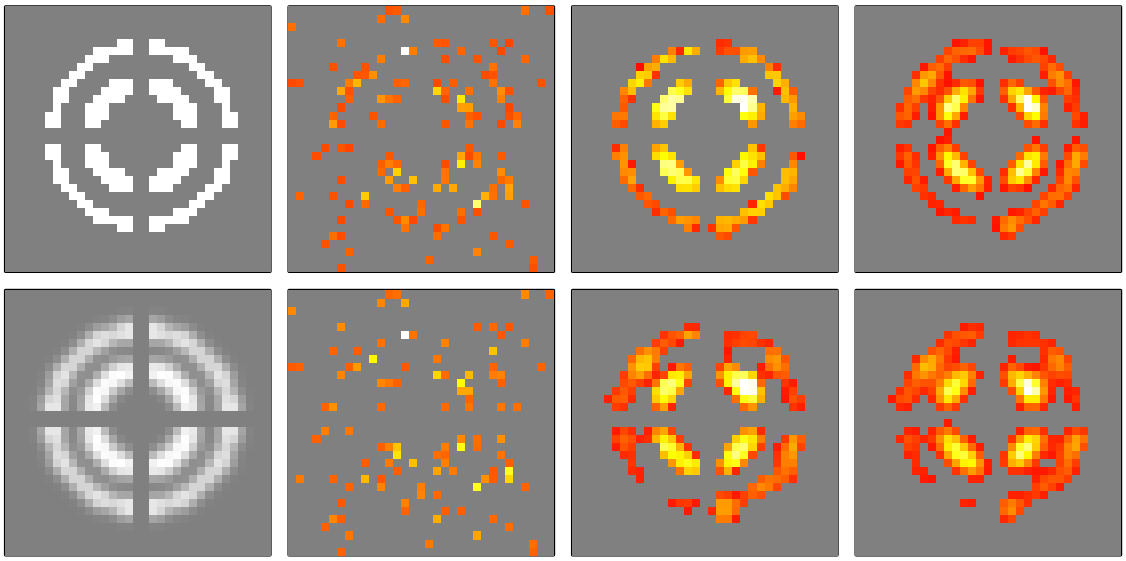

Figure 2: Analysis of an artificial fMRI experiment shown in a central slice (from left to right): a) Signal size for the expected BOLD response assigned to the voxel. In the upper row of images an indicator function was used for the signal strength, while in the lower row this function is smooth in radial direction. b) Result of a voxelwise analysis without smoothing, which produces a large portion of false positives. On the other hand, if thresholds are controlled by a global significance level the analysis generally fails to detect many if not all activations. c) Result of an analysis using the adaptive smoothing procedure (PS) described in this paper. We see almost no false positive activations (see Figure 3 for details) and some none detected voxel. d) In contrast to this the result of an analysis using non-adaptive smoothing shows an oversmoothed border of the activation areas. Gaps between areas are only partly preserved in case of non-adaptive smoothing.

activation areas rather than over-smoothing them.

4.2 Application to real data

With the results of the preceeding section in mind we now consider real fMRI-data. The images were acquired at Citigroup Biomedical Imaging Center, Weill Medical College of Cornell University on a GE 3T scanner using 2D gradient echo EPI sequence with TE/TR = 40/2000 ms. 26 axial slices of 4mm thickness and a matrix size of 64×64 were acquired. Task were performed in three blocks during 3.7 min of scanning time. The task for the data presented here was right hand finger tapping. After reconstruction of the raw data and motion correction, we analyzed the data. In Figure 4 we compare the results of this analysis in selected slices using non adaptive smoothing (upper row) and adaptive smoothing (PS). It can be clearly seen that the two results differ in the detection of activation areas. The

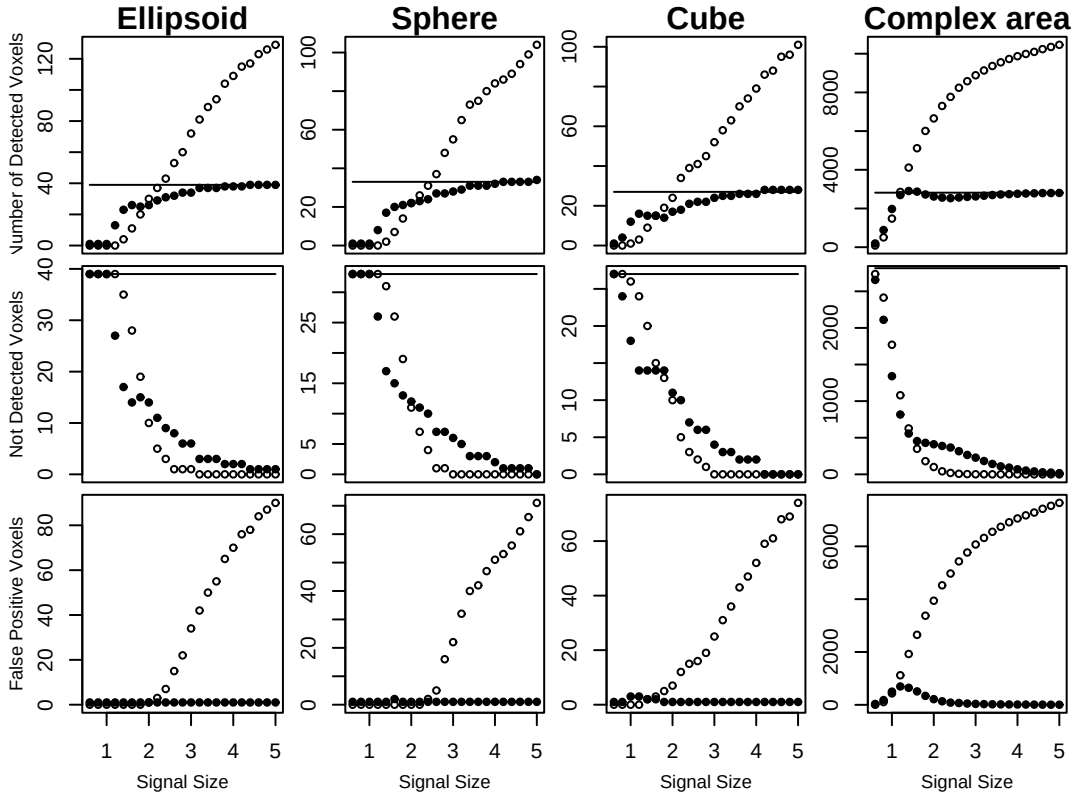

Figure 3: Analysis of artificial data for several shapes of the activation area (from left to right): ellipsoid, sphere, cube, and configuration from Figure 2. Signal size is increasing from 0.6 to 5 (x-axis). The upper row illustrates the dependence of the number of detected voxel on signal size. Circles and bullets correspond to non adaptive and adaptive smoothing, respectively. The (maximum) bandwith is chosen according to the size of the activation area. The line indicates the true number of active voxel. The second row shows the number of not detected voxel. In the lower row the corresponding number of false positives is provided.

non adaptive smoothing procedure shows the typical effects of applying a gaussian filter. In contrast to this adaptive smoothing leads to a more detailed shape of the activation areas. Having the results of our analysis of artificial data and the theoretical properties of propagation separation method Polzehl and Spokoiny (2005) in mind, we conclude, that the latter reveals the shape and extend of the activation area.

Additionally the density of the estimated signals $\widetilde{\gamma}$ from (1) in detected voxel differs for voxel detected using adaptive and non adaptive smoothing, respectively. Figure 5 illustrates this providing densities of $\widetilde{\gamma}$ for detected voxel (left plot) and voxel detected by only one method (right plot). Note that the mean of $\widetilde{\gamma}$ over voxel detected exclusively using adaptive smoothing is much larger than the corresponding quantity using non-adaptive

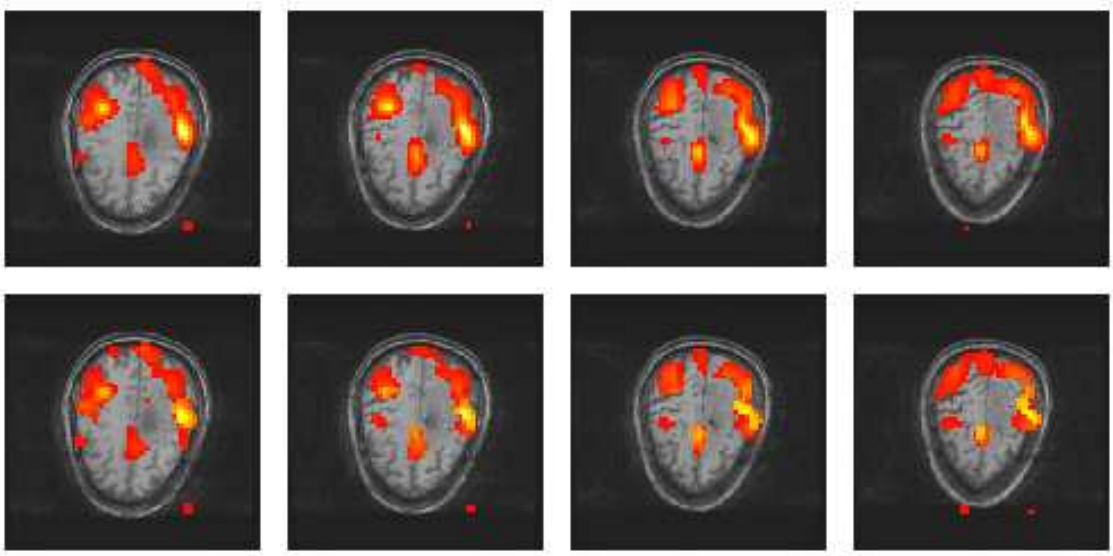

Figure 4: **fMRI**: Illustration of fMRI data from a right hand finger tapping experiment. Signal detection for real fMRI data. Slices 17–20. Upper row: nonadaptive smoothing with bandwidth (FWHM) $h = 13.2mm$, Lower row: adaptive smoothing with maximal bandwidth (FWHM) $h = 13.2mm$ showing a much better recognition of shape of activation areas. Data: H. Voss, Citigroup Biomedical Imaging Center, Weill Medical College of Cornell University.

smoothing.

Finally we demonstrate the effect of considering local thresholds, see Subsection 3.7. We first estimate the correlation at some voxel from the achieved amount of variance reduction and then calculate a local threshold according to Random Field Theory using the expected Euler Characteristic according to (8). This procedure takes into account, that due to the border preserving properties of the adaptive smoothing method the effective bandwidth achieved in the smoothing process is less than the maximum bandwidth and varies locally. The density of such a local threshold is shown in Figure 6 and compared with the global threshold obtained for non-adaptive smoothing employing bandwidth h_{max}.

5 Summary

In this paper we present a general approach to integrate adaptive smoothing into the analysis of fMRI experiments. While, compared to the use of Gaussian filtering, reaching a similar amount of noise reduction and sensitivity, information on shape and geometry of the activation areas is preserved. While the basic idea of the Propagation-Separation approach has already been discussed in Polzehl and Spokoiny (2005) we show how this can be

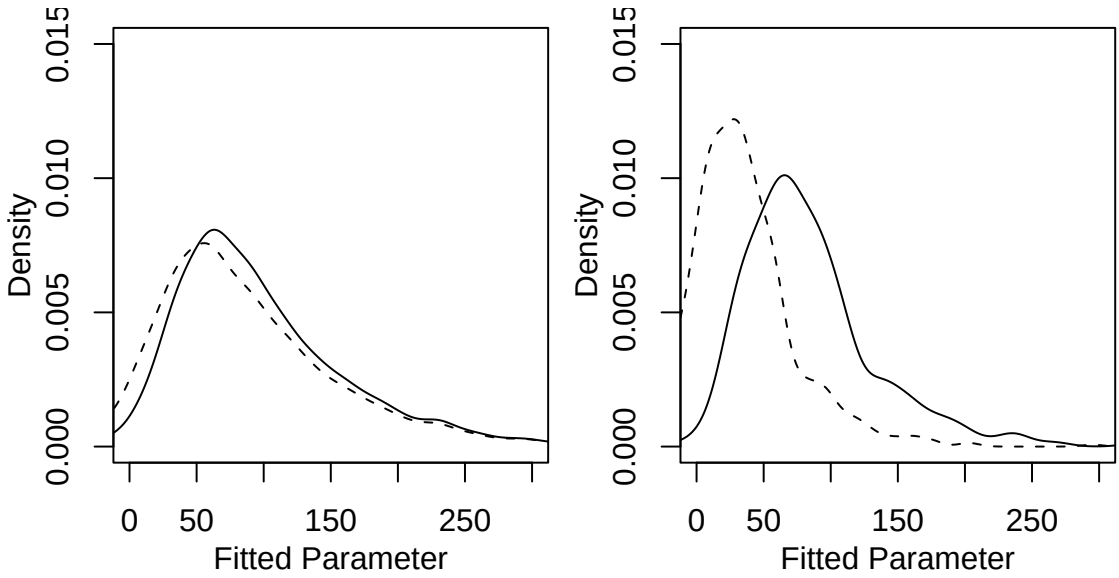

Figure 5: The density of the estimated parameters $\widetilde{\gamma}$ for all detected voxel (left) and for voxel detected only by the specified method (right). The dashed line corresponds to non adaptive smoothing while the solid line is the result from adaptive smoothing.

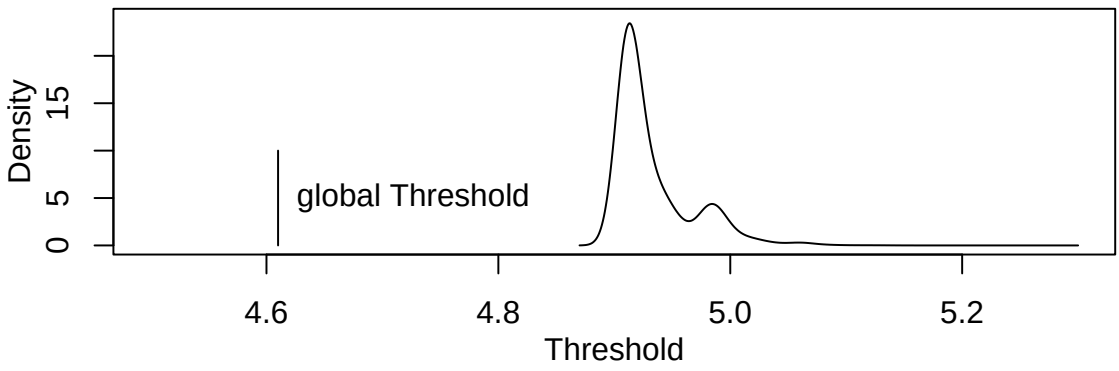

Figure 6: Density of local thresholds given by (8) for a global significance level of 0.05 and global threshold for non-adaptive smoothing for FWHM bandwidth $h = h_{max} = 3.52\, v_x\ mm$.

extended for spatially correlated data. We take the local correlation structure into account to define corresponding local thresholds using Random Field Theory. Finally we show, that smoothing the map of estimated parameters instead of estimating the parameters from smoothed images increases the number of degrees of freedom. Hence the array $\widehat{\Theta}$ is well approximated by a Gaussian field.

We foresee a variety of application. Presurgical planning for tumor resection involves fMRI experiments for important functions. Since EPI images of the tumor can be made with high resolution it is of considerable interest to reach a similar level on spatial information to properly decide the extend of activation areas and possible invasion of the tumor. The results will be published elsewhere Tabelow et al. (2005).

6 Acknowledgments

This work is supported by the DFG Research Center MATHEON in project A3. We thank H. Voss from the Citigroup Biomedical Imaging Center, Weill Medical College of Cornell University for providing the fMRI data used in this paper.

References

Glover, G. H. (1999). Deconvolution of impulse response in event-related bold fmri. *NeuroImage*, 9:416–429.

Kiebel, S. J., Poline, J. B., Friston, K. J., Holmes, A., and Worsley, K. J. (1999). Robust smoothness estimation in statistical parametric maps using standardized residuals from the general linear model. *NeuroImage*, 10:756–766.

Lange, N. (1996). Statistical approaches to human brain mapping by functional magnetic resonance imaging. *Stat. in Medicine*, 15:389–428.

Lange, N. and Zeger, S. (1997). Non-linear fourier time series analysis for human brain mapping by functional magnetic resonance imaging. *J. Roy. Statist. Soc. Ser. C*, 46:1–29.

Polzehl, J. and Spokoiny, V. (2000). Adaptive weights smoothing with applications to image restoration. *J. Roy. Statist. Soc. Ser. B*, 62:335–354.

Polzehl, J. and Spokoiny, V. (2001). Functional and dynamic magnetic resonance imaging using vector adaptive weights smoothing. *J. Roy. Statist. Soc. Ser. C*, 50:485–501.

Polzehl, J. and Spokoiny, V. (2005). Propagation-separation approach for local likelihood estimation. *Probab. Theory Relat. Fields*, in print.

Purdon, P. L., Solo, V., Weisskoff, R. M., and Brown, E. (2001). Locally regularized spatiotemporal modeling and model comparison for functional mri. *NeuroImage*, 14:912–923.

Rosenfeld, A. and Kak, A. (1982). *Digital picture processing*, volume 2. Academic Press, Orlando.

Tabelow, K., Polzehl, J., Spokoiny, V., Ulug, A., Dyke, J., Heier, L. H., and Voss, H. (2005). Accurate localization of functional brain activity using structure adaptive smoothing. (in preparation).

Worsley, K. (1994). Local maxima and the expected euler characteristic of excursion sets of χ^2, f and t fields. *Advances in Applied Probability*, 26:13–42.

Worsley, K. (2002). Non-stationary fwhm and its effect on statistical inference of fmri data. *NeuroImage*, 15:346.

Worsley, K. (2005). Spatial smoothing of autocorrelations to control the degrees of freedom in fmri analysis. *NeuroImage*, 26:635–641.

Worsley, K., Andermann, M., Koulis, T., MacDonald, D., and Evans, A. (1999). Detecting changes in non-isotropic images. *Human Brain Mapping*, 8:98–101.

Worsley, K., Liao, C., Aston, J. A. D., Petre, V., Duncan, G., Morales, F., and Evans, A. (2002). A general statistical analysis for fmri data. *NeuroImage*, 15:1–15.

Worsley, K., Marrett, S., Neelin, P., and Evans, A. (1996a). Searching scale space for activation in pet images. *Human Brain Mapping*, 4:74–90.

Worsley, K., Marrett, S., Neelin, P., Friston, K., and Evans, A. (1996b). A unified statistical approach for determing significant signals in images of cerebral activation. *Human Brain Mapping*, 4:58–73.